PERGAMON

International Journal of Heat and Mass Transfer 41 (1998) 4139–4150

International Journal of HEAT and MASS TRANSFER

Physico-chemical processes occurring inside a degrading two-dimensional anisotropic porous medium

Colomba Di Blasi*

Dipartimento di Ingegneria Chimica, Universitá degli Studi di Napoli Federico II Piazzale V. Tecchio, 80125 Napoli, Italy

Received 7 July 1997; in final form 31 March 1998

Abstract

A lumped-parameter kinetic model is applied to simulate the pyrolysis of lignocellulosic particles, exposed to a high temperature environment. Physical processes account for radiative, conductive and convective heat transport, diffusion and convection of volatile species and pressure and velocity variations across a two-dimensional (2-D), anisotropic, variable property medium. The dynamics of particle degradation are found to be strongly affected by the grain structure of the solid. A comparison is made between the total heat transferred to the virgin solid (conduction minus convection) along and across the grain. Notwithstanding the lower thermal conductivities, because of the concomitant slower convective transport (lower gas permeabilities), the largest contribution is that across the solid grain. The role played by convective heat transport is successively less important as the particle size is increased. Finally, the 2-D and the widely applied one-dimensional (1-D) predictions are compared.

Nomenclature

A_i pre-exponential factor [s^{-1}]
B permeability [m^2]
c heat capacity [kJ kg^{-1} K^{-1}]
d pore diameter [m]
e surface emissivity
E_i activation energy [kJ mol^{-1}]
k thermal conductivity [W mK^{-1}]
p gas pressure [N m^{-2}]
q_r enthalpy variation due to chemical reactions [kW m^{-3}]
Q heat flux [equations (25)–(27)]
r reaction rate [kg m^{-3} s^{-1}]
R universal gas constant
t time [s]
t_c conversion time [s]
T temperature [K]
T_r furnace temperature [K]
u gas velocity (x) [m s^{-1}]
v gas velocity (y) [m s^{-1}]
V volume [m^3]
W_g mean molecular weight
x space [m]
X_S solid mass fraction
y space [m].

Greek symbols
Δh enthalpy variation [kJ kg^{-1}]
ε porosity
η [equation (20)]
μ viscosity [kg m^{-1} s^{-1}]
v yield coefficient (% by weight of cellulose)
ρ mass concentration [kg m^{-3}]
σ Stefan–Bolzmann constant
τ particle half-thickness (x, y) [m]
ω emissivity.

Subscripts
A active solid
C char
G gas
g total volatiles (gas + tar)
i ith chemical species
k kth chemical reaction
S solid
T tar
W solid (wood)
0 ambient value.

* Corresponding author. Tel.: 39 081 768 2232.

0017–9310/98 $19.00
PII: S0017–9310(98)00142–2

1. Introduction

Wood pyrolysis is a problem of interest in the field of solid fuel flammability and biomass thermochemical conversion. Indeed, the fire behavior of solids is characterized by two main parts [1]: the solid phase problem (composition and rate of generation of fuel vapors from the degrading solid) and the gas phase problem (oxidation of the devolatilization products with flaming combustion). In the field of energy recovery from biomass and municipal solid wastes [2, 3], pyrolysis is an independent methodology, widely investigated, to obtain gaseous, liquid or charred fuels. It is also a fundamental step in gasification technology, following solid drying and preceding char combustion and gasification. For both fields, pyrolysis is a complex process dominated by a strong interaction between transport phenomena and chemical reactions.

Basic process characteristics have been investigated mainly with reference to single-particle systems. In order to simplify the understanding of the problem, experiments have been often conducted under 1-D flow and heat conditions. Wood cylinders [4, 5], cellulosic cylinders [6] and wood spheres [7] have been placed in furnaces heated, with an assigned rate, to final temperatures varying from about 550–920 K. In other cases [8–11] wood cylinders have been uniformly heated on the top side with radiative flux intensities varying from about 21–250 kW m^{-2}. The measurements available give the time history of temperature at different radii [6, 7] or different stations along the axis [4, 5, 8–11] of the sample, mass loss weight and, in a few cases, the pressure profiles [5, 8] or the rough composition of evolved products [9–11].

The modeling literature on the pyrolysis of lignocellulosic materials has been reviewed recently [12]. In the meanwhile, some comprehensive models [13–18] have also been proposed where multi-step pyrolysis schemes, including primary and secondary pyrolysis reactions, have been coupled to the description of the main physical processes. Again, these mathematical formulations apply to one-dimensional flow and heat conditions. However, wood is an anisotropic material with different properties along, across and tangential to the grain [19]. Thermal conductivity across and tangential to the grain direction is approximately one third that along the grain. Also, the permeability to gas flow across the wood grain is much lower than that along the other two directions (up to a factor of 10^4).

In this study a two-dimensional, unsteady model of a single particle (sample) pyrolysis is presented to give an adequate description of the anisotropic structure of lignocellulosic materials and to quantify its implications in the pyrolytic degradation. The influence of heat transfer mechanisms is investigated on the structure of the pyrolysis front and global pyrolysis characteristics, such as conversion time, mass loss rate and product yields. Two-dimensional predictions are compared, when appropriate, with the widely used one-dimensional theories.

2. Mathematical model

Chemical reactions of lignocellulosic materials, exposed to high temperature sources in an inert atmosphere, can be roughly classified as primary and secondary [12]. Primary reactions are concerned with the degradation of the solid into char and numerous volatile products, whereas secondary reactions are those undergone by primary volatile products. From the chemical point of view, the degradation of lignocellulosic materials is a very complex process, involving hundreds of products. However, notwithstanding the application of rather sophisticated experimental techniques since the early 1960s [20], a comprehensive understanding of this chemistry is still far from being achieved. On the other hand, the application of detailed kinetics of lignocellulosic materials together with the description of the complex physical processes could give rise to mathematical formulations unaffordable from the computational point of view. Lumped-parameter models [12] offer a valuable alternative, as they generally account for the main competitive chemical pathways and the formation of the three main classes of products, char (the solid residual), gas (low molecular weight gaseous species: mainly CO, CO_2, H_2 and C_1–C_2 hydrocarbons) and liquid tars (all condensable, high molecular weight, organic components). However, reliable kinetic data for such mechanisms formulated for wood degradation are not available [12], whereas cellulose has been widely investigated. Therefore, in this study the primary degradation of cellulose is used to model the thermal response of lignocellulosic materials (the most recent reviews of the kinetics of cellulose pyrolysis are presented in [21, 22]). This approach is considered valid because cellulose and hemicellulose account for about 75% of wood composition (cellulose (c. 50%), hemicellulose (c. 25%), the remaining part being lignin) and, even though these components exhibit different thermal stability characteristics, some similarity exists between their kinetics of degradation. The mechanism here considered is known as the Broido–Shafizadeh scheme and has been successfully applied in one-dimensional simulations [14, 15, 17, 18]:

$$SOLID \xrightarrow{K_1} ACTIVE\ SOLID \begin{cases} \xrightarrow{K_3} TAR \\ \xrightarrow{K_2} \nu_C CHAR + \nu_G GAS \end{cases}$$

This mechanism accounts for the formation of an active solid with a reduced degree of polymerization and two competing reaction pathways, (a) intermolecular dehydration, predominating at low temperatures, leading

to char and gas and, in air to smoldering combustion; and (b) depolymerization reaction, predominating at high temperatures, leading to tar and, in air, to flaming combustion. Reactions are endothermic and their rates are represented as first order in the mass of pyrolyzable material and with an Arrhenius type of temperature dependence. Secondary reactions of primary pyrolysis products and gasification of char are not taken into account, because the analysis is mainly focused on physical processes. On the other hand, some aspects of their effects on process dynamics and product yields have already been investigated [13].

From the physical point of view, the model here presented describes the transport phenomena occurring through the cross (square) section of a lignocellulosic sample exposed in a pre-heated, inert atmosphere furnace. To study the effects of wood anisotropy on the thermal degradation, different properties along the x and y directions are assigned (corresponding to those across and along the wood grain). Because of the symmetry of the problem, only one fourth of the sample is considered, according to the schematic reported in Fig. 1.

The formulation of the mathematical model is based on the following main assumptions:

(1) constant total volume occupied by the cell wall sample as the solid undergoes pyrolysis, that is, no thermal swelling and/or shrinkage and surface regression (the effects of 1-D particle shrinkage on pyrolysis characteristics have been discussed in [16]),
(2) local thermal equilibrium between the solid matrix and the volatiles (the volumetric solid heat capacity is much larger than that of the gas phase and, as volatile products flow, they are rapidly heated to the temperature of the char [12]),
(3) no condensation of tar, if any migrates through the cold solid (one-dimensional simulations [13] indicate that this process does not occur to a significant extent),
(4) negligible moisture content (moisture evaporation can significantly affect pyrolysis characteristics; model extension to include these effects is currently under way [23]).

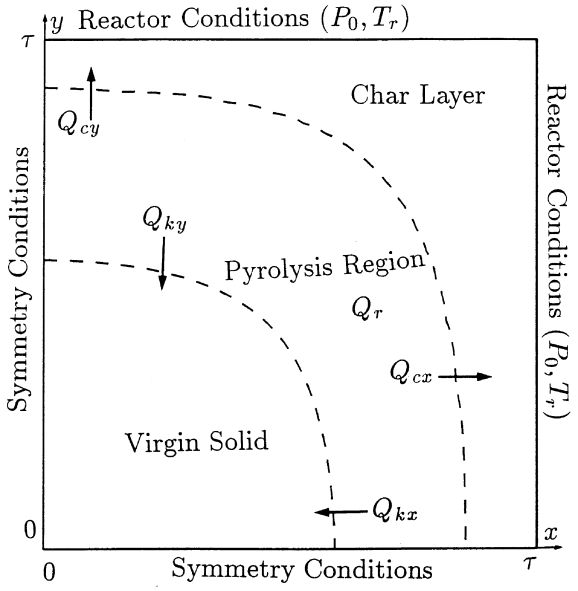

Fig. 1. Schematic of the solid degradation problem.

Physical processes described include:

(1) radiative, convective and conductive heat transfer interior to the solid and from the exposed surfaces,
(2) momentum transfer to account for non zero pressure gradients and non uniform velocity,
(3) variable properties (thermal conductivity, porosity and permeability vary linearly with the conversion level, from the initial wood to the final char values),
(4) accumulation of volatile energy and mass in the pores of the solid,
(5) volatile transport through the pores of both the virgin solid and the charred region.

Thus the unsteady, 2-D mathematical model includes equations for:

—virgin solid

$$\frac{\partial \varrho_W}{\partial t} = -r_1 \tag{1}$$

—active intermediate solid

$$\frac{\partial \varrho_A}{\partial t} = r_1 - r_2 - r_3 \tag{2}$$

—solid char

$$\frac{\partial \varrho_C}{\partial t} = \nu_C r_2 \tag{3}$$

—total gas-phase continuity

$$\frac{\partial(\varepsilon\varrho_g)}{\partial t} + \frac{\partial(\varrho_g u)}{\partial x} + \frac{\partial(\varrho_g v)}{\partial y} = \nu_G r_2 + r_3 \tag{4}$$

—enthalpy

$$(\varrho_C c_C + \varrho_W c_W + \varrho_A c_A + \varepsilon\varrho_g c_g)\frac{\partial T}{\partial t} + \varrho_g c_g u\frac{\partial T}{\partial x} + \varrho_g c_g v\frac{\partial T}{\partial y} = \frac{\partial}{\partial x}\left(k_x^*\frac{\partial T}{\partial x}\right) + \frac{\partial}{\partial y}\left(k_y^*\frac{\partial T}{\partial y}\right) + q_r \tag{5}$$

—momentum (the multi-dimensional Darcy law)

$$u = -\frac{B_x}{\mu}\frac{\partial p}{\partial x}, \quad v = -\frac{B_y}{\mu}\left(\frac{\partial p}{\partial y} + \varrho_g g\right). \tag{6–7}$$

Also, the ideal gas law and a linear variation of the solid-phase volume with the conversion level are considered:

$$p = \frac{\varrho_g RT}{W_g} \tag{8}$$

$$\frac{V_s}{V_{s0}} = \frac{(\varrho_W + \varrho_C + \varrho_A)}{\varrho_{W0}}. \quad (9)$$

In the formulation of equations (1)–(9) the following definitions are used:

$$K_i = A_i \exp(-E_i/RT) \quad i = 1, 3 \quad (10)$$

$$r_1 = A_1 \exp(-E_1/RT)\varrho_W$$

$$r_i = A_i \exp(-E_i/RT)\varrho_A, \quad i = 2, 3 \quad (11)$$

$$\varrho_W = M_W/V, \quad \varrho_C = M_C/V,$$

$$\varrho_g = M_g/V_g = M_g/(\varepsilon V) \quad (12\text{–}14)$$

$$\varepsilon = V_g/V, \quad V_g = V - V_S \quad (15\text{–}16)$$

$$q_r = K_1\varrho_W[\Delta h_1 + (T - T_0)(c_W - c_A)] + K_2\varrho_A[\Delta h_2 + (T - T_0)(c_A - v_C c_C - v_G c_G)] + K_3\varrho_A[\Delta h_3 + (T - T_0)(c_A - c_T)] \quad (17)$$

$$k_x^* = \eta k_{Wx} + (1-\eta)k_{Cx} + \varepsilon k_g + \sigma T^3 d_x/\omega,$$

$$k_y^* = \eta k_{Wy} + (1-\eta)k_{Cy} + \varepsilon k_g + \sigma T^3 d_y/\omega \quad (18)$$

$$B_x = \eta B_{Wx} + (1-\eta)B_{Cx}, \quad B_y = \eta B_{Wy} + (1-\eta)B_{Cy} \quad (19)$$

$$\eta = (\varrho_A + \varrho_W)/\varrho_{W0}. \quad (20)$$

Initially, the sample is at ambient conditions and is suddenly exposed in an inert atmosphere, where the pressure is p_0 and the temperature is T_r. Boundary conditions are written as:

$$x = \tau : k_x^* \frac{\partial T}{\partial x} = -e\sigma(T^4 - T_r^4) - h_c(T - T_r), \quad p = p_0 \quad (21)$$

$$y = \tau : k_y^* \frac{\partial T}{\partial y} = -e\sigma(T^4 - T_r^4) - h_c(T - T_r), \quad p = p_0 \quad (22)$$

(at the other two sides, $x = 0$, and $y = 0$, symmetry conditions are imposed).

The numerical solution of equations (1)–(9) with initial and boundary conditions, is computed through a finite difference formulation of the model equations, based on the hybrid scheme, already applied for the simulation of the 2-D structure of smoldering combustion through packed beds [24] and flame spread over charring solids [25].

3. Results

The properties used in the numerical simulations describe a lignocellulosic fuel. The kinetic data, the values of the heat of pyrolysis and the medium properties are the same as in [14–18]: $A_1 = 2.8 \times 10^{19}\ s^{-1}$, $A_2 = 1.3 \times 10^{10}\ s^{-1}$, $A_3 = 3.28 \times 10^{14}\ s^{-1}$, $E_1 = 242.4$ kJ mol^{-1}, $E_2 = 150.5$ kJ mole^{-1}, $E_3 = 196.5$ kJ mole^{-1}, $v_G = 0.65$, $v_C = 0.35$, $\Delta h_1 = 0$, $\Delta h_2 = \Delta h_3 = -418$ kJ kg^{-1}, $\rho_{W0} = 400$ kg m^{-3}, $c_W = c_A = 2.3$ kJ kg^{-1} K^{-1}, $c_g = 1.8$ kJ kg^{-1} K^{-1}, $c_C = 1.1$ kJ kg^{-1} K^{-1}, $d_x = d_y = 4 \times 10^{-5}$ m, $k_g = 25.77 \times 10^{-3}$ W mK^{-1}, $\mu = 3 \times 10^{-5}$ kg/ms, $\omega = 1$, $h_c = 20$ W K^{-1} s^{-1}. Thermal conductivities are taken from [8] and permeabilities have been estimated so as to give gas overpressures of the same order as those experimentally observed [8]. Values along the x and y directions are chosen to describe cross (low values) and parallel (high values) grain properties: $B_{Wx} = B_{Ax} = 1 \times 10^{-14}$, $B_{Cx} = 5 \times 10^{-12}$, $B_{Wy} = B_{Ay} = 1 \times 10^{-11}$, $B_c = 5 \times 10^{-11}$ m^2; $k_{Wx} = k_{Ax} = 10.5 \times 10^{-2}$, $k_{Cx} = 7.1 \times 10^{-2}$, $k_{Wy} = k_{Ay} = 25.5 \times 10^{-2}$, $k_{Cy} = 10.46 \times 10^{-2}$ W m^{-1} K^{-1}. This set of data will be referred to as reference data. The particle, at the initial temperature of 300 K, is suddenly exposed in a high temperature furnace (900 K). Simulations have been made for anisotropic (square) particles by varying their sizes, from $\tau = 0.25 \times 10^{-2}$ m to $\tau = 3 \times 10^{-2}$ m. Simulations have also been made for isotropic particles, to understand the role played by the different mechanisms, and two-dimensional and one-dimensional results compared.

3.1. Dynamics of wood particle pyrolysis

An example of the dynamics of the degradation process is presented for $\tau = 0.5 \times 10^{-2}$ m, by means of the constant contour levels of temperature, the variable η (equation (20), a measure of particle conversion), gas overpressure and reaction rate ($r_3 = K_3\varrho_A$) and the gas vector velocity field (Figs 2(A–D), 3(A–D), 4(A–D), the whole cross section of the sample is considered for an easier understanding of the problem). Profiles of temperature, char density and velocity (u and v, respectively) along the x and y axes (directions perpendicular and parallel to the solid grain, respectively) are plotted in Fig. 5(A–C). From the qualitative point of view, the process dynamics show the same characteristics as already simulated by 1-D models [14]. The usual regions of virgin solid, pyrolysis and charred residual are seen. The virgin solid is followed by an elevated pressure zone due to slow transport (convection and diffusion) of volatiles in a region of low porosity and permeability to gas flow. However, the 2-D simulations show that the shape of the temperature, pressure and reaction fronts, for fixed external conditions, is dictated by the anisotropy of the medium.

The reaction process is initially localized along the external boundary of the sample and, as time increases, it assumes a wave-like character (Fig. 2(A–D)). The pyrolysis region, here defined by the contours of η equal to 0.01 and 0.99, is characterized by temperature values varying from 700 K (side of the char layer) to about 600 K (virgin solid side). As can be observed from the contours of the rate of reaction (3) (Fig. 3(A–D)) and the conversion level, the reaction fronts propagate, with decreasing rate, towards the center of the sample. The increasing distance from the exposed surfaces causes progressively lower maximum values of the reaction rate and an enlargement of the thickness of the reaction zone,

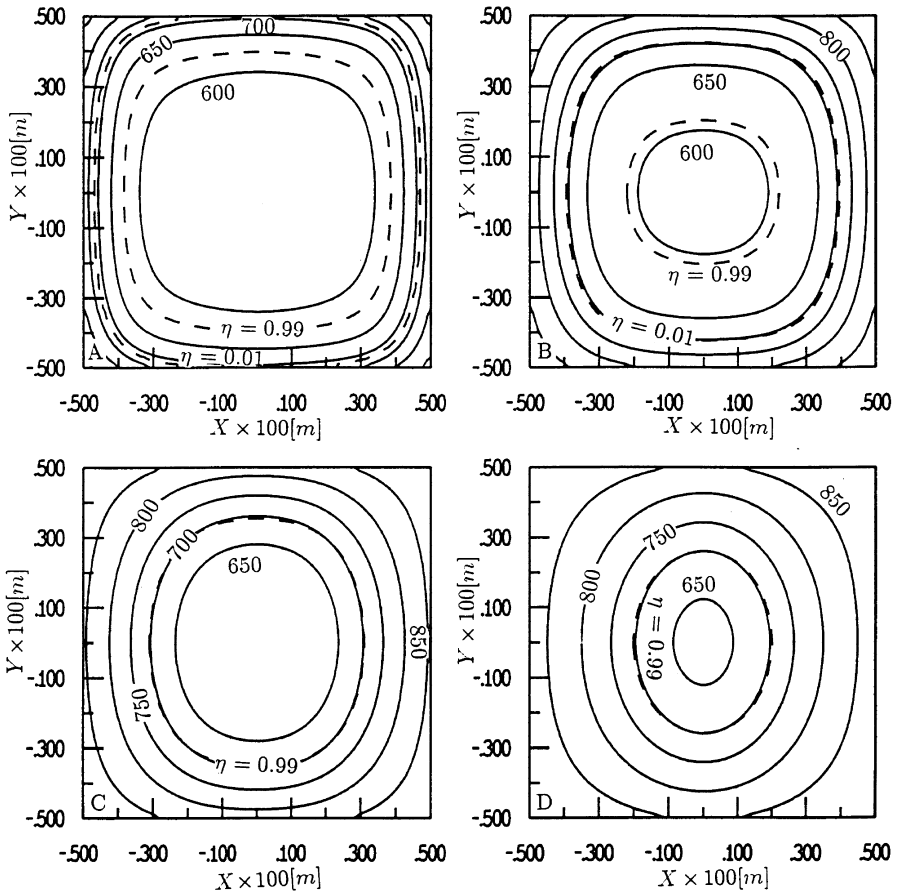

Fig. 2. Isotherms [K] (solid lines, step equal to 50) and constant contour levels of η (dashed lines) for $t = 31$ s (A), 63 s (B), 93 s (C) and 125 s (D).

until for $t > 80$ s particle heat-up occurs, that is, the pyrolysis region extends to the whole particle. The rate of advancement of the charring and devolatilization fronts through the virgin solid is, for very short times, faster for the cross grain direction. This is because the surface heat flux is always larger for this direction, though the difference with the parallel grain surface heat flux continuously decreases. It should be noted that, for very slow furnace heating rates and sufficiently small samples, this feature may be observed until complete conversion. In the case of a sample instantaneously exposed to the final furnace temperature, apart from the very beginning of the process, the position of the pyrolysis front is slightly more advanced along the solid grain. However, the thickness of the pyrolysis region is also much larger for this direction. Thus, complete charring is, on the whole, slower along the solid grain and, for times longer than that of particle heat-up, the shape of the reaction zone becomes ellipsoidal.

The temperature distribution is responsible for such behavior. Indeed, Fig. 2(A–D) shows that the temperature field closely resembles the shape of the reaction front. On the other hand, from Fig. 5(A), it appears that temperatures, along the two directions, are comparable for the virgin solid and the pyrolysis regions, whereas, they are significantly larger across the grain for the char layer.

The different thermal history of the degrading solid along the x and y directions also exerts some influence on the chemical pathways. As indicated by the lower activation energy, reaction (2) (char and gas formation) is favored at low temperatures. As can be observed from Fig. 5(B), char densities increase with the distance from the exposed surfaces (progressively lower reaction temperatures) and are larger along the solid grain (lower temperatures). Furthermore, as already observed, the devolatilization rate is initially faster across the grain (for $t \leqslant 20$ s), but for longer times, the onset of the pyrolysis process occurs at about the same time for the two directions.

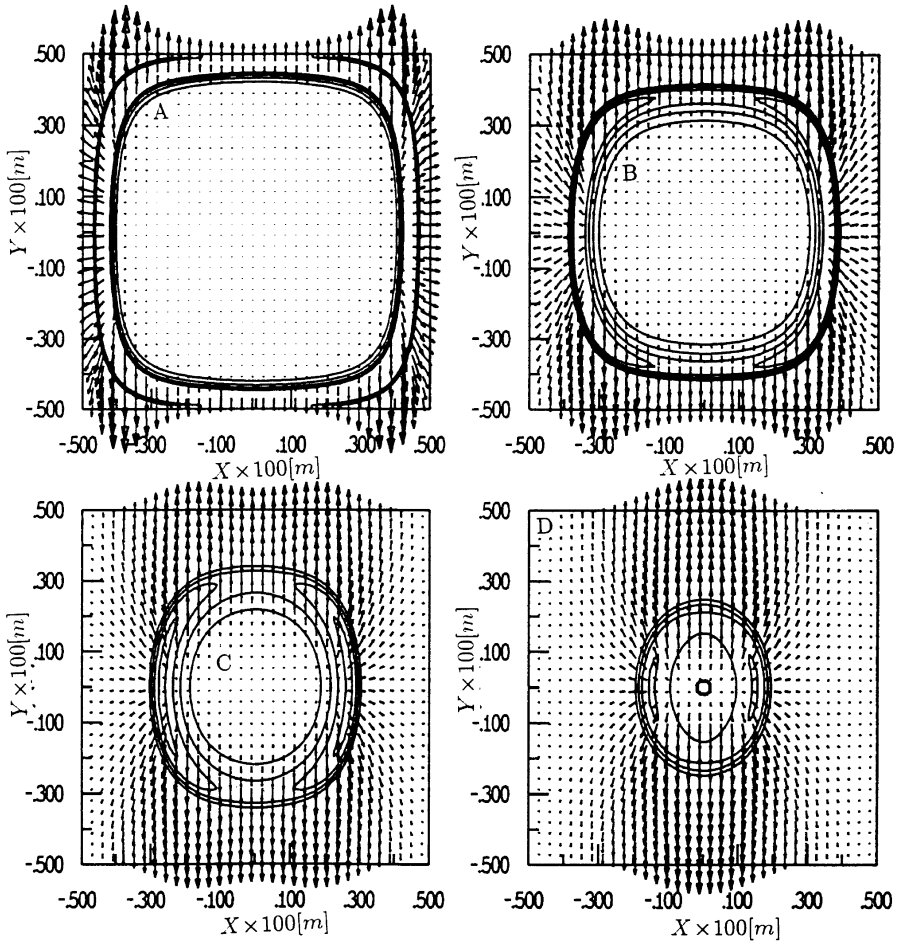

Fig. 3. Constant contour levels of reaction rate [kg m^{-3} s^{-1}] from 1 and then with step 1 and vector velocity field for the same times as Fig. 2. Maximum vector velocity [m s^{-1}]: 0.126 (A), 0.095 (B), 0.08 (C) and 0.09 (D).

The grain structure of the solid strongly affects the flow of volatile pyrolysis products through the pores. Thermal degradation is initially faster in the neighborhood of the right boundary, that is across the grain (Figs 2(A–D) and 5(C)). Thus, for short times, a significant mass outflow is observed along this region. However, since the char permeability to gas flow is larger along the grain, much higher values of the mass efflux are reached through a narrow region of the upper boundary, close to the vigorous pyrolysis zone. The formation of volatile products in a partially reacted medium (pyrolysis region), where porosity and permeability are still low, and the migration of volatile products towards the unreacted solid both cause the pressure to increase across a rather wide zone, parallel to the solid grain (Fig. 4(A–D)).

As time increases and significant degradation takes place also along the grain direction, volatile products flow mostly along this direction and escape from the upper boundary. In accordance with the wave-like character of the process, the gas overpressure front propagates towards the centerline of the sample and, as with the reaction fronts, enlarges. The flow velocity, which is the result of the volatile release rate and pressure gradients, initially attains successively lower values as degradation proceeds, because of the continuously decreasing reaction temperatures. For very long times, very slow volatile flow is observed from the right boundary, while there is an increase of the mass escaping from the upper boundary, as a consequence of the attainment of particle heat-up conditions. Finally, very slow velocities directed towards the cold solid are simulated.

The time of complete sample conversion is 144 s and char represents 4.4% of the initial weight of the solid. As char and gas productions are linked, it can be inferred

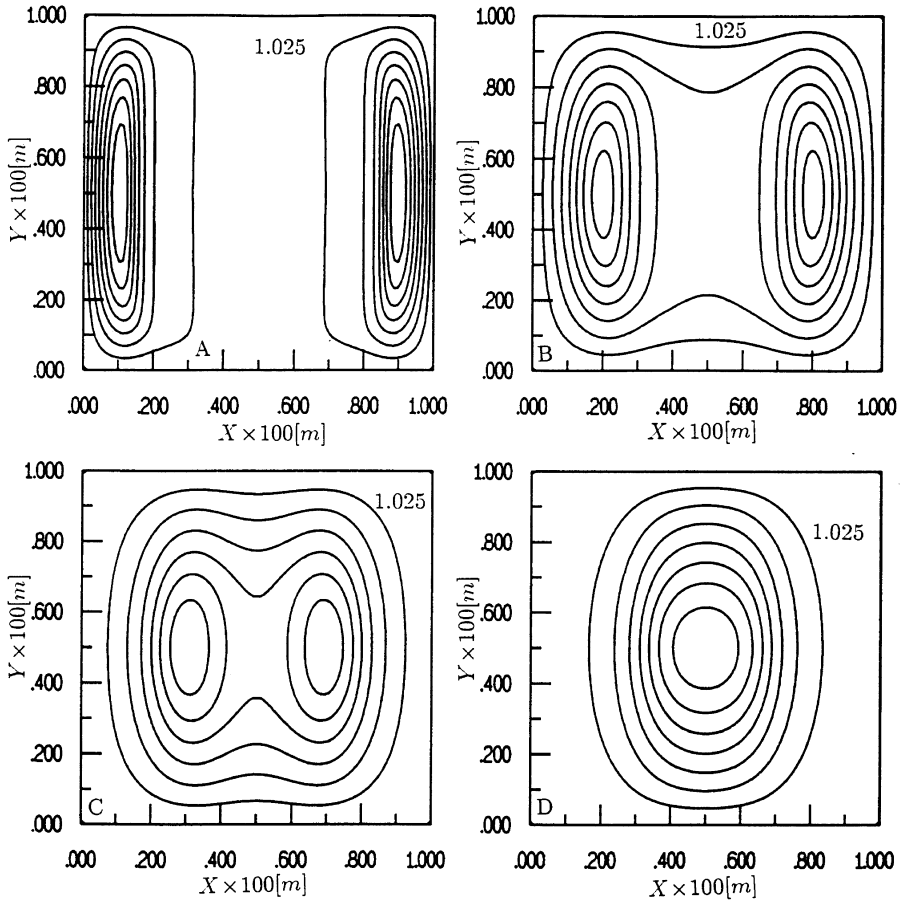

Fig. 4. Constant contour levels of gas overpressure p/p_0 from 1 and with step 0.025 for the same times as Fig. 2.

that primary gas yield is 8.14%, the remaining amount of volatiles being tar.

To further clarify the influence of the anisotropy in the permeability to gas flow on the temperature distribution, simulations have also been made with no anisotropy in this property, for both high (no pressure variations) and low values. As expected, the velocity field becomes symmetric, so that convective transport of heat and mass is quantitatively about the same along the two directions with the maximum value reduced by a factor of about two. However, in terms of global parameters, the process is not significantly different from the reference case. It can be guessed that, given the higher flow velocity simulated by the reference data, the volatile residence times are shorter. Consequently, some influence can be expected on the extent of the activity of secondary reactions, not modeled in this study. Finally, it should be noted that, in the absence of convective heat transport, the conversion time becomes shorter (125 s) and the char yields are also slightly lower (4.2%).

3.2. Relative importance of the different heat transfer mechanisms

Some general considerations can be drawn from the process dynamics here presented. The slow flow of hot pyrolysis products pre-heats the virgin solid making the rate of primary pyrolysis faster. On the contrary, transport of hot volatile products towards the charred surface cools the pyrolysis region. The formation of a thick low thermal conductivity char layer also hinders heat conduction from the exposed surface to the interior of the solid. Given that the solid is porous, radiation could be another mode of heat transfer, mainly along the char and pyrolysis regions where rather high temperatures are reached (this contribution is, however, small for the case here considered). In order to evaluate the role played by the different heat transfer mechanisms during the conversion process, the enthalpy equation is integrated over the computational domain to get:

$$H_i = Q_{kx} - Q_{cx} + Q_{ky} - Q_{cy} + Q_r \tag{23}$$

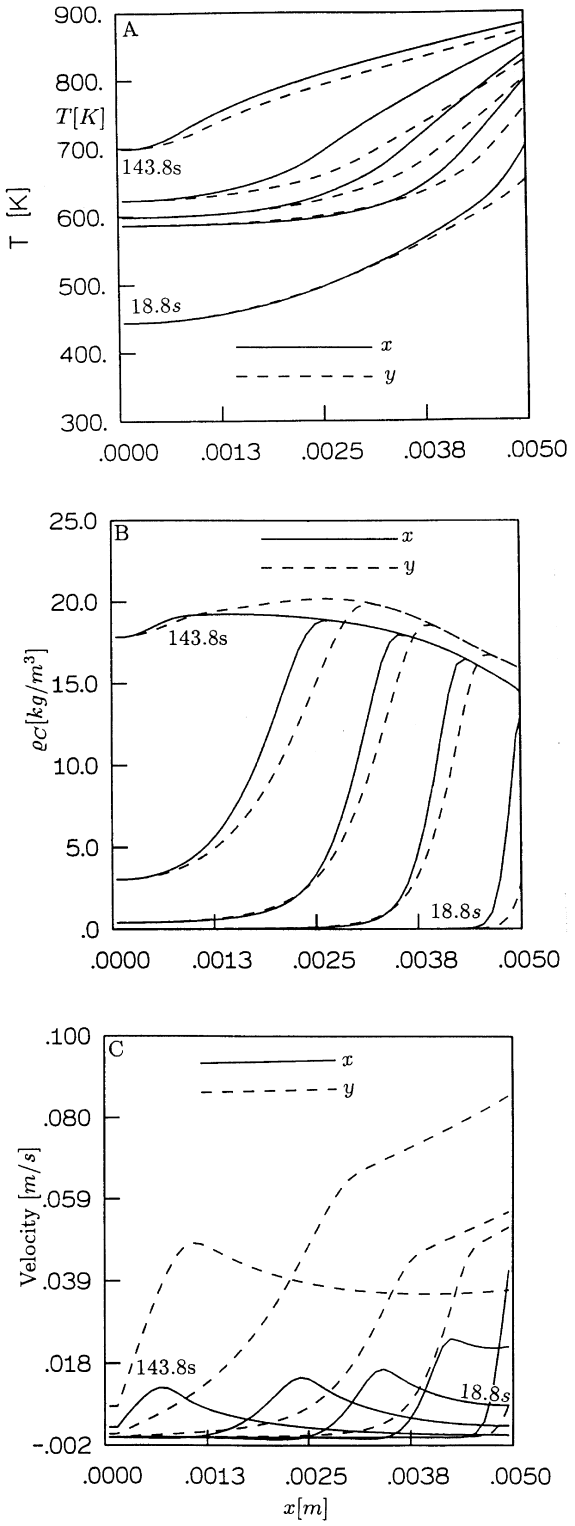

Fig. 5. Profiles along the axis x ($y = 0$, solid lines) and y ($x = 0$, dashed lines) of temperature (A), char density (B) and velocity (C, u and v, respectively) from $t = 18.8$ s and then with step 31 s.

where Q_{kx} and Q_{ky} are the contributions due to conduction (x, y), Q_{cx} and Q_{cy} those due to convection (x, y) and Q_r the heat needed for the reactions to occur (Fig. 1). They can be detailed as follows:

$$H_i = \int_0^{\tau}\int_0^{\tau}\left((c_W\varrho_W + c_A\varrho_A + c_C\varrho_C + \varepsilon c_g\varrho_g)\frac{\partial T}{\partial t}\right)\mathrm{d}y\,\mathrm{d}x \tag{24}$$

$$Q_{kx} = \int_0^{\tau}\left(k_x^*\frac{\partial T}{\partial x}\right)_{x=\tau}\mathrm{d}y, \quad Q_{ky} = \int_0^{\tau}\left(k_y^*\frac{\partial T}{\partial y}\right)_{y=\tau}\mathrm{d}x, \tag{25}$$

$$Q_{cx} = \int_0^{\tau}(uc_g\varrho_g(T-T_0))_{x=\tau}\,\mathrm{d}y,$$

$$Q_{cy} = \int_0^{\tau}(vc_g\varrho_g(T-T_0))_{y=}\,\mathrm{d}x \tag{26}$$

$$Q_r = \int_0^{\tau}\int_0^{\tau}(q_r)\,\mathrm{d}y\,\mathrm{d}x. \tag{27}$$

The contributions (25)–(27) are reported in Fig. 6 as functions of time (as the reaction process is globally endothermic, to use the same scale, $-Q_r$ is plotted). Q_{ky} is always larger than Q_{kx} and both of them decrease as time increases owing to the temperatures at the surface approaching the final furnace temperature. Q_r attains its maximum (negative) value during the initial stages of the degradation process, when the resistance to heat transfer is low, and then continuously decreases. Interesting is also the time dependence of the heat convected out by the pyrolysis products. In agreement with the degradation process previously described, Q_{cx} is initially slightly larger

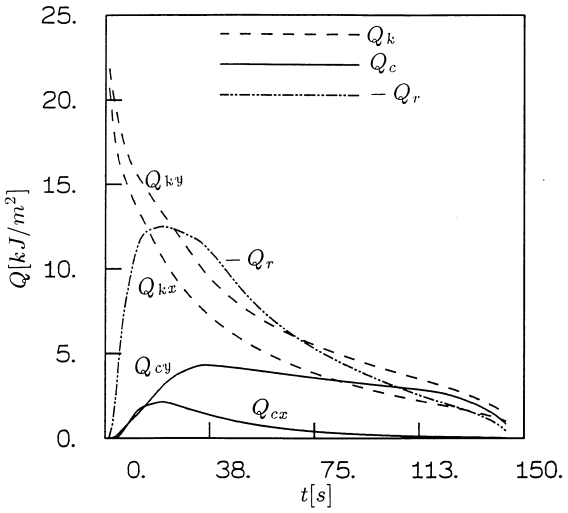

Fig. 6. Q_{kx}, Q_{ky}, Q_{cx}, Q_{cy} and $-Q_r$ as functions of time for $T_r = 900$ K and $\tau = 0.5\times10^{-2}$ m.

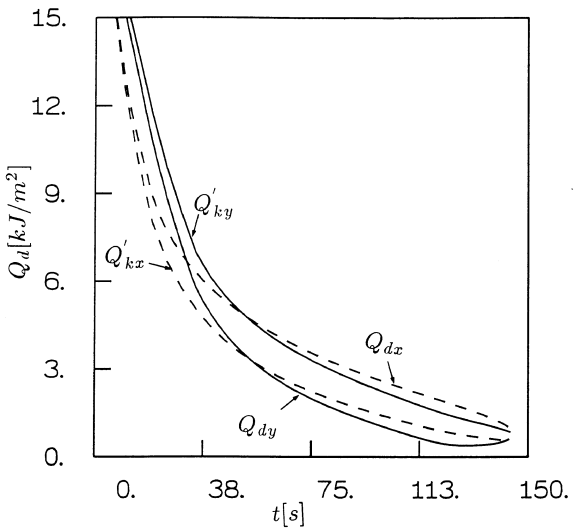

Fig. 7. Q'_{kx}, Q'_{ky} (cross grain permeability values for both the x and y direction), Q_{dx} and Q_{dy} (reference data) as functions of time for $T_r = 900$ K and $\tau = 0.5 \times 10^{-2}$ m.

than Q_{cy}, but rapidly decays to very low values. On the contrary, Q_{cy} assumes rather large values as long as the solid is undergoing pyrolysis. Thus convective transport of heat along the solid grain plays a role of increasing importance for long times when conductive transport values become lower. Indeed, the integral forces driving heat transfer interior to the solid are: $Q_{dx} = Q_{kx} - Q_{cx}$ and $Q_{dy} = Q_{ky} - Q_{cy}$.

The contributions Q_{dx} and Q_{dy} are reported in Fig. 7 as functions of time. It appears that, for $t \geqslant 38$ s, the integral contribution to inward heat transfer is larger for the x direction (across the grain). In the same figure, a comparison can be made with the equivalent net integral forces driving heat interior to the solid for the same pyrolysis process simulated for comparable values of the convective heat transport along the two directions (that is, for the cross grain values of permeability along both the x and y direction), that is Q'_{kx} and Q'_{ky}. In this case the heat transferred along the solid grain (y) is always larger than that transferred across the x direction, because of the larger thermal conductivities. As expected, during the transients of the process, Q'_{ky} is larger than Q_{dy}, and Q'_{kx} lower than Q_{dx}, because, in the symmetric case, convective transport is reduced along the grain and increased across the grain, when compared with the reference case.

3.3. Comparison between 2-D and 1-D simulations

The temperature, char density and velocity profiles along the two axes [x (cross grain direction) and y (parallel grain direction)] simulated by the 2-D model (Fig. 5(A–C)) can be compared with the corresponding 1-D simulations shown in Fig. 8(A–C). For short times ($t < 20$ s), the 2-D and the 1-D simulations produce results quantitatively close. However, for longer times, significant differences appear from both the qualitative and the quantitative points of view. For the cross grain direction, 1-D predictions show slightly lower temperatures and comparable velocities, with respect to the 2-D case. As a consequence of the lower temperatures, the propagation rate of the charring front is slower and the final char density higher (mainly for long times). The 1-D, parallel grain profiles exhibit temperatures larger and velocities lower (these by a factor of about two) than the corresponding 2-D simulations, for most part of the process. Consequently, the 1-D charring front propagates faster and shows lower char densities. A change in this trend is seen for times longer than that of particle heat-up. In fact, because of the faster propagation rate, 1-D solid conversion occurs at temperatures lower, on average, and final char densities become larger.

These results indicate that the multi-dimensional structure of the pyrolysis front affects not only the profiles of dependent variables but also global parameters, such as conversion time and product yields, though the differences are not exceedingly large. In fact, conversion times are 142.5 s and 200 s (against 144 s of the 2-D case) and char yields 4.9 and 5.2% (against 4.44% of the 2-D case), for the 1-D parallel and perpendicular grain heating, respectively.

The global dynamics of sample conversion, as its size is varied, can be observed from Fig. 9, where the solid weight loss and the rate of weight loss are plotted as functions of time. For all cases, an initial period of slow weight loss is observed, this being most noticeable for the larger samples. For small sizes, a fast rise in the rate of solid devolatilization, due to fast attainment of temperatures high enough for solid degradation, is followed by a decrease, due to the process becoming heat transfer controlled. For large particles, the dynamics of devolatilization remain qualitatively the same, but the process is much slower and the peak in the time derivative of the solid weight becomes successively less evident.

The isolines of η (pyrolysis region) and the vector velocity field, for three different particle sizes and conversion conditions of 50%, are shown in Fig. 10(A–C). The configurations are qualitatively similar. That is, for all the sizes here considered, the conversion process appears to be under the heat transfer control [17]. As expected, the spatial gradients increase and the maximum velocities decrease, as the size is made larger. Thus convective transport becomes successively less important, because the higher resistance to internal heat transfer causes reductions in the global devolatilization rates. The process is on the whole slowed and, given that the temperatures at the reaction fronts are, on average, successively lower, char formation is also successively more favored.

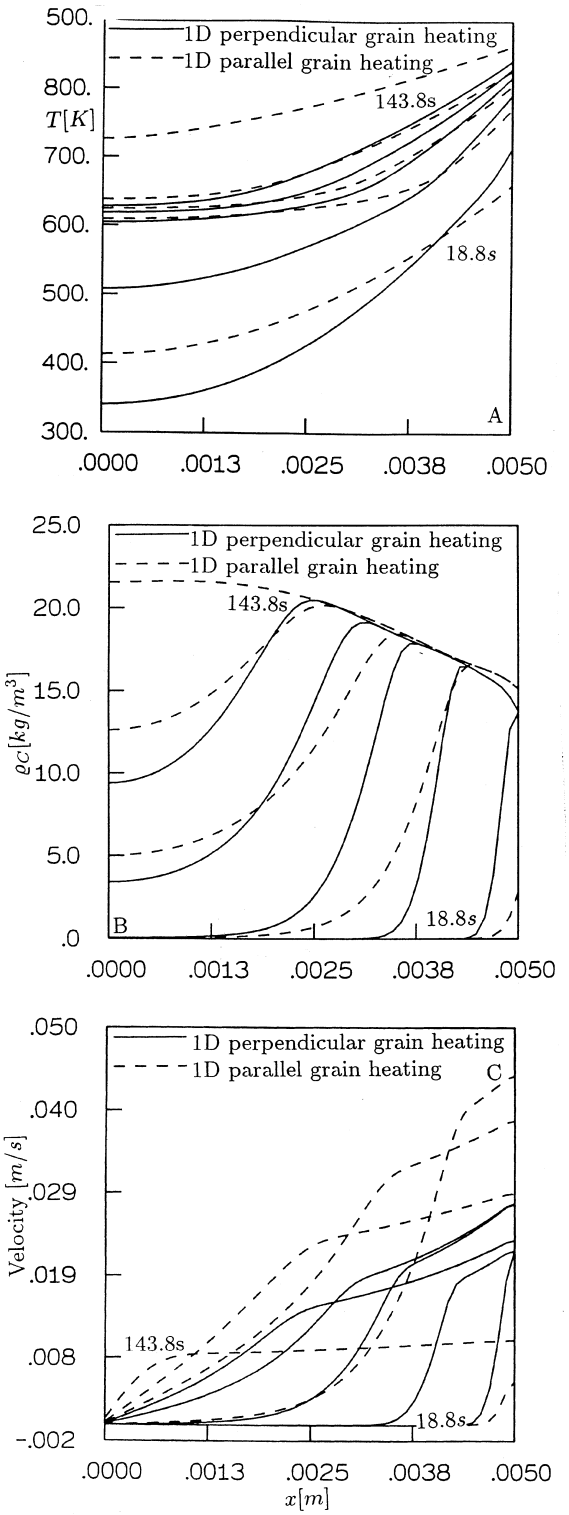

Fig. 8. Profiles (1-D simulations) for perpendicular (solid lines) and parallel (dashed lines) grain heating of: temperature (A); char density (B); and velocity (C) from $t = 18.8$ s and then with step 31 s.

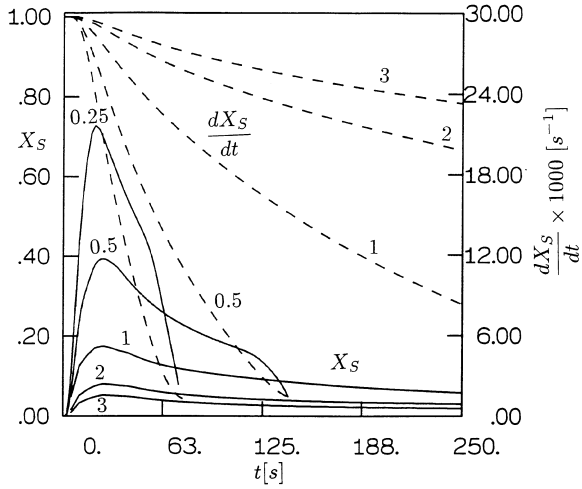

Fig. 9. Weight fraction (dashed lines) and time derivative of the weight fraction (solid lines) as functions of time for several values of the particle size ($\tau \times 100$ [m], reported in the figure).

Final char yields and conversion times, as predicted by the 1-D and the 2-D model, are reported in Fig. 11 as functions of the sample size. In qualitative agreement with experiments [9, 26, 27] and as expected from the detailed variable distributions, char yield and conversion time increase with the particle size, for both models. Though the large number of parameters and the large uncertainty about values and dependence on conversion conditions make any quantitative comparison between predictions and experimental results difficult, good agreement has been obtained by the 1-D version of the model in [16, 17, 23]. On the other hand, a comparison of 2-D numerical simulation results with experimental data is not made at this stage because detailed measurements of the two-dimensional structure of pyrolysis fronts are not available. The 2-D model predicts, on average, larger temperatures at the reaction front, so that particle conversion is faster and gives rise to lower solid char yields. The differences between the two mathematical formulations tend to become larger with the particle size. It should be noted, however, that in all cases the 2-D and 1-D (parallel grain heating) conversion times are nearly the same.

4. Conclusions

Two-dimensional, unsteady balance equations for chemical species, energy and momentum have been used to simulate the pyrolysis of a lignocellulosic, anisotropic material. Model predictions have been carried out to understand the role of physical mechanisms in the pyrolysis of samples of different sizes.

For high external temperatures, typical of ther-

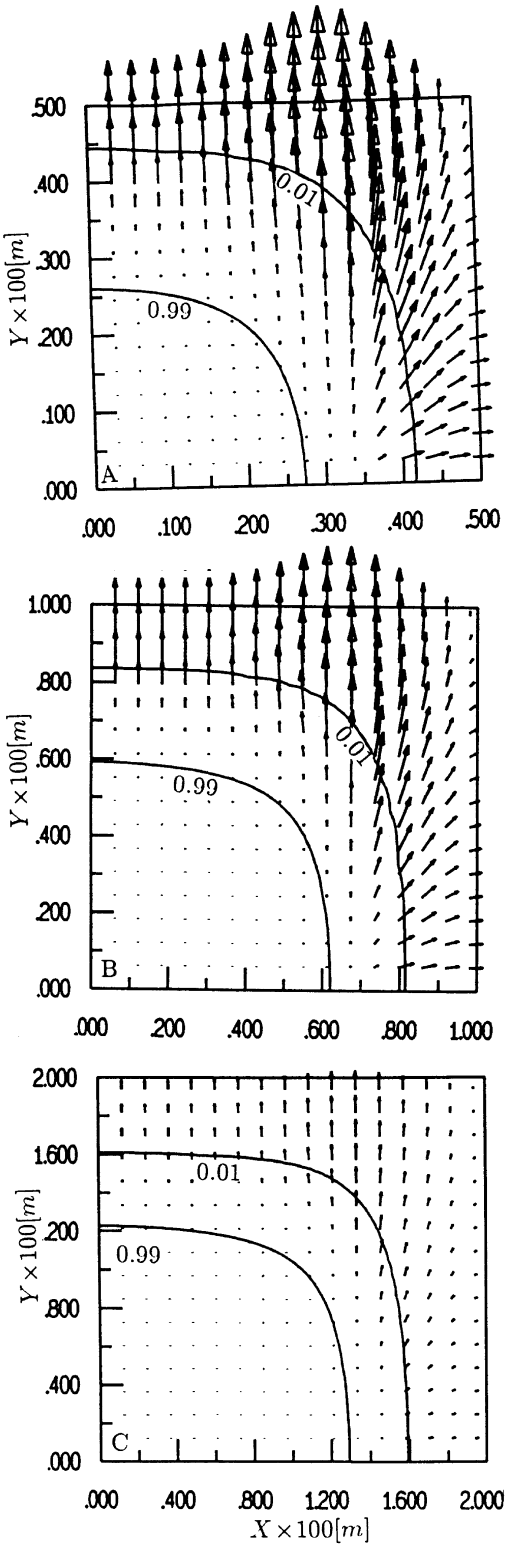

Fig. 10. Constant contour levels of η and vector velocity field for three particle sizes and conversion of 50%. Maximum vector velocity [m s^{-1}]: 0.10 (A), 0.068 (B), and 0.038 (C).

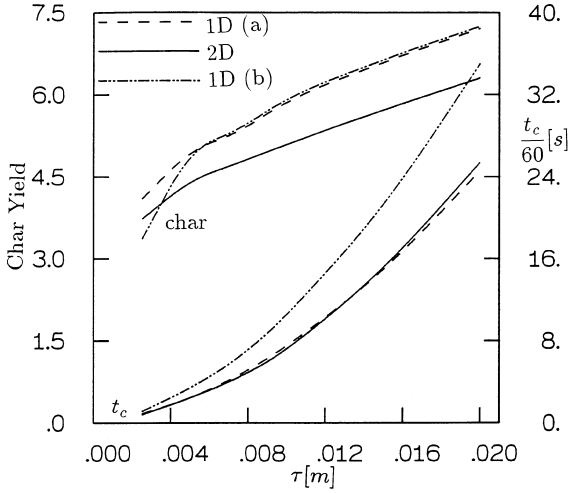

Fig. 11. Conversion time and final char yields, as simulated by the 2-D model and 1-D model (parallel (a) and perpendicular (b) grain heating), as functions of the sample size.

mochemical conversion and fire conditions, the pyrolysis process is heat transfer controlled and presents a wave-like character with the propagation of pressure and reaction fronts from the heat exposed surface towards the interior of the sample. The rate of advance of these fronts is highly affected by the grain structure of the solid.

The relative importance of the convective and conductive heat transfer mechanisms along and across the grain directions has been assessed. It has been found that, notwithstanding the lower thermal conductivities, because of the concomitant slower convective transport (lower permeabilities to gas flow), the largest contribution is that across the solid grain. However, the contribution due to volatile convection is successively less important as the size of the sample is increased.

A comparison between the 2-D and the 1-D simulations has shown that the multi-dimensional structure of the reaction fronts affects not only the details of sample conversion dynamics, but also global parameters, such as conversion time and product distribution. On average, the process is faster and the volatiles yields larger for the 2-D configuration. This finding should be taken into consideration when comparing 1-D theories with experiments. Indeed, truly 1-D systems can be designed and operated only on a laboratory, single-particle scale, while the reaction processes undergone by particles in fixed and fluidized gas–solid reactors or by lignocellulosic structures under fire conditions are multi-dimensional.

Acknowledgement

The work was supported by the European Economic Community under Contract AIR2-CT93-0889.

References

[1] M.A. Kanury, Thermal decomposition kinetics of wood pyrolysis, Combustion and Flame 18 (1972) 75–83.

[2] M.A. Kanury, Combustion characteristics of biomass fuels, Combustion Science and Technology 97 (1994) 469–491.

[3] A.V. Bridgwater, Catalysis in thermal biomass conversion, Applied Catalysis A: General 116 (1994) 5–47.

[4] A.F. Roberts, G. Clough, Thermal decomposition of wood in an inert atmosphere, Ninth International Symposium on Combustion 1963, pp. 158–166.

[5] E.R. Tinney, The combustion of wooden dowels in heated air, Tenth International Symposium on Combustion 1965, pp. 925–930.

[6] A.M. Kanury, P.L. Blackshear, An X-ray photographic study of the reaction kinetics of α-cellulose decomposition, Pyrodynamics 4 (1966) 285–297.

[7] R. Bilbao, A. Millera, M.B. Murillo, Temperature profiles and weight loss in the thermal decomposition of large spherical wood particles, Ind. Eng. Chem. 32 (1993) 1811–1817.

[8] C.K. Lee, R.F. Chaiken, J.M. Singer, Charring pyrolysis of wood in fires by laser simulation, Sixteenth International Symposium on Combustion. The Combustion Institute, Pittsburgh, 1976, pp. 1459–1470.

[9] W.R. Chan, M. Kelbon, B. Krieger-Brockett, Single-particle biomass pyrolysis: correlation of reaction products with process conditions, Ind. Eng. Chem. Res. 27 (1988) 2261–2275.

[10] T.J. Ohlemiller, T. Kashiwagi, K. Werner, Wood gasification at fire level heat fluxes, Combustion and Flame 69 (1987) 155–170.

[11] T. Kashiwagi, T.J. Ohlemiller, K. Werner, Effects of external radiant flux and ambient oxygen concentration on nonflaming gasification rates and evolved products of white pine, Combustion and Flame 69 (1987) 331–345.

[12] C. Di Blasi, Modeling and simulation of combustion processes of charring and non-charring solid fuels, Progress in Energy and Combustion Science 19 (1993) 71–104.

[13] C. Di Blasi, Analysis of convection and secondary reaction effects within porous solid fuels undergoing pyrolysis, Combustion Science and Technology 90 (1993) 315–339.

[14] C. Di Blasi, Numerical simulation of cellulose pyrolysis, Biomass and Bioenergy 7 (1994) 87–98.

[15] C. Di Blasi, Influences of model assumption is on the predictions of cellulose pyrolysis in the heat transfer controlled regime, Fuel 75 (1996) 58–66.

[16] C. Di Blasi, Heat, momentum and mass transfer through a shrinking biomass particle exposed to thermal radiation, Chemical Engineering Science 51 (1996) 1121–1132.

[17] C. Di Blasi, Kinetic and heat transfer control in the slow and flash pyrolysis of solids, Ind. Eng. Chem. Res. 35 (1996) 37–46.

[18] C. Di Blasi, Heat transfer mechanisms and multi-step kinetics in the ablative pyrolysis of cellulose, Chemical Engineering Science 51 (1996) 2211–2220.

[19] J.F. Siau, Transport Processes in Wood, Springer-Verlag, Berlin, 1984.

[20] M.J. Antal, Biomass pyrolysis: a review of the literature. Part 1—carbohydrate pyrolysis, in: K.W. Boer, J.A. Duffie (Eds), Advances in Solar Energy, American Solar Energy Society, Boulder, CO, 1 (1982) 61–111.

[21] M.J. Antal, G. Varhegyi, Cellulose pyrolysis kinetics: the current state of knowledge, Ind. Eng. Chem. Res. 34 (1995) 703–717.

[22] I. Milosavlijevic, E.M. Suuberg, Cellulose thermal decomposition kinetics: global mass loss kinetics, Ind. Eng. Chem. Res. 34 (1995) 1081–1091.

[23] C. Di Blasi, Multi-phase moisture transfer in the high-temperature drying of wood particles, Chemical Engineering Science 53 (1998) 353–366.

[24] C. Di Blasi, Mechanisms of two-dimensional smoldering propagation through packed fuel beds, Combustion Science and Technology 106 (1995) 103–124.

[25] C. Di Blasi, Predictions of unsteady flame spread and burning processes by the vorticity-stream function formulation of the compressible Navier–Stokes equations, International Journal of Numerical Methods for Heat and Fluid Flow 5 (1995) 511–529.

[26] M.R. Hajaligol, J.B. Howard, J.P. Longwell, W.A. Peters, Product compositions and kinetics for rapid pyrolysis of cellulose, Ind. Eng. Chem. Process Des. Dev. 21 (1981) 457–465.

[27] D.S. Scott, J. Piskorz, M.A. Bergougnou, R. Graham, R.P. Overend, The role of temperature in the fast pyrolysis of cellulose and wood, Ind. Eng. Chem. Res. 27 (1988) 8–15.

[28] Di Blasi C, Russo G. Modeling of transport phenomena and kinetics of biomass pyrolysis, in: A.V. Bridgwater (Ed.), Proceedings of the International Conference on Advances in Thermochemical Biomass Conversion, Blackie A.&P., 1994, pp. 906–921.